Syngas Production from H_2O and CO_2 over Zn Particles in a Packed-bed Reactor

Anastasia Stamatiou and Peter G. Loutzenhiser
Dept. of Mechanical and Process Engineering, ETH Zurich, Zurich 8092, Switzerland

Aldo Steinfeld
Dept. of Mechanical and Process Engineering, ETH Zurich, Zurich 8092, Switzerland
Solar Technology Laboratory, Paul Scherrer Institute, Villigen 5232, Switzerland

DOI 10.1002/aic.12580
Published online March 28, 2011 in Wiley Online Library (wileyonlinelibrary.com).

The solar thermochemical production of H_2 and CO (syngas) from H_2O and CO_2 is examined via a two-step cycle based on Zn/ZnO redox reactions. The first, endothermic step is the thermolysis of the ZnO driven by concentrated solar energy. The second, nonsolar step is the exothermic reaction of Zn with a mixture of H_2O and CO_2 yielding syngas and ZnO; the latter is recycled to the first step. A series of experimental runs of the second step was carried out in a packed-bed reactor where ZnO particles provided an effective inert support for preventing sintering and enabling simple and complete recycling to the first, solar step. Experimentation was performed for Zn mass fractions in the range of 33–67 wt % Zn-ZnO, and inlet gas concentrations in the range 0–75% H_2O–CO_2, yielding molar Zn-to-ZnO conversions up to 91%. A 25 wt % Zn-ZnO sample mixture produced from the solar thermolysis of ZnO was tested in the same reactor setup and exhibited high reactivity and conversions up to 96%. © 2011 American Institute of Chemical Engineers *AIChE J,* 58: 625–631, 2012
Keywords: energy, reactor analysis

Introduction

The production of syngas from H_2O and CO_2 using Zn/ZnO redox reactions in a two-step thermochemical cycle provides a promising path for converting solar energy into a storable and dispatchable form, as syngas is the precursor to liquid hydrocarbon fuels.[1,2] The cycle is carbon-neutral when coupled to processes to capture CO_2 from air.[3] The first step of the cycle is the highly endothermic reaction driven by concentrated solar energy, given as

$$\mathrm{ZnO} \rightarrow \mathrm{Zn} + \frac{1}{2}\mathrm{O_2} \qquad \Delta H^{\circ}_{298\,\mathrm{K}} = 350.5\,\mathrm{kJ\,mol^{-1}} \qquad (1)$$

which has been experimentally demonstrated with a 10 kW solar reactor.[4,5] Solar Zn can also be produced via solar thermal electrolysis of ZnO,[6] and solar carbothermal reduction of ZnO.[7] The second, nonsolar step is the exothermic reaction of CO_2 and H_2O with Zn, given as

$$\mathrm{Zn} + \beta\mathrm{CO_2} + (1-\beta)\mathrm{H_2O} \rightarrow \mathrm{ZnO} + \beta\mathrm{CO} + (1-\beta)\mathrm{H_2}$$
$$-108.8\,\mathrm{kJ\,mol^{-1}} < \Delta \mathrm{H}^{\circ}_{298\,\mathrm{K}} < -67.5\,\mathrm{kJ\,mol^{-1}} \qquad (2)$$

with $0 < \beta < 1$. The ZnO is then recycled to the first step for a net reaction $\beta CO_2 + (1-\beta)H_2O \rightarrow \beta CO + (1-\beta)H_2 + \frac{1}{2}O_2$. In contrast to the direct thermolysis of CO_2 and H_2O, the two-step cycle bypasses the need to separate gaseous products. Other redox metal oxides cycles, especially those based on ferrites and ceria, have been investigated for H_2O and CO_2-splitting thermochemical cycles.[8–17]

Previous works have examined various chemical aspects of the second step, including identification of reaction

Correspondence concerning this article should be addressed to A. Steinfeld at aldo.steinfeld@ethz.ch.

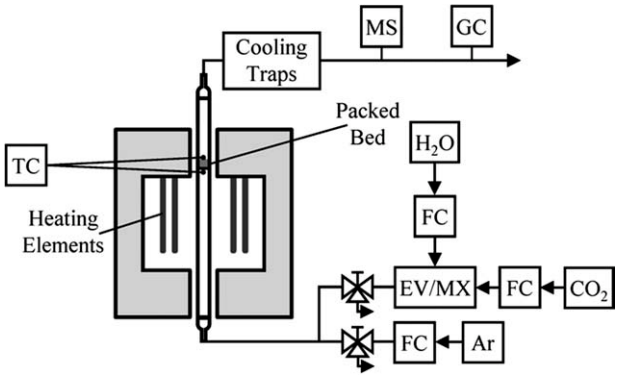

Figure 1. Scheme of packed-bed reactor setup.

mechanisms and determination of kinetic parameters for the reaction of Zn with H_2O[18–23] or CO_2.[24] Competitive reactions of Zn with both H_2O and CO_2 were modeled using Langmuir-Hinshelwood kinetics.[25,26] Aerosol flow reactors have been applied for quenching Zn(g) to form nanoparticles that react *in situ* with CO_2 or H_2O.[27–33] These configurations offered high Zn-to-ZnO conversions over short residence times due to augmented reaction kinetics and heat/mass transfer. However, the reactions primarily occurred heterogeneously outside the aerosol jet flow on surfaces with Zn deposition, making the ZnO recovery, process control and scale-up problematic. Laboratory studies were performed with steam bubbling through molten zinc,[34] but the continuous removal of ZnO(s) may pose additional process complications. As for the cyclability of the Zn/ZnO redox reactions, no changes in the behavior are expected with cycling because ZnO(s) undergoes a phase change to Zn(g) during the first (solar) reduction step and the particles are regenerated each time by condensation.

A novel, packed-bed reactor containing mixtures of Zn and ZnO particles[35] was successfully demonstrated with Zn-to-ZnO conversions as high as 77%. Mixtures of Zn and ZnO particles served as an effective inert support for preventing sintering and enabled simple and complete recovery of ZnO particles for recycling to the first, solar step after experimentation. The reactor concept is extended in this work to investigate the concurrent CO_2 and H_2O reductions for the direct syngas production with commercial Zn/ZnO mixtures and solar Zn resulting from Eq. 1. The effects of the H_2O/CO_2 concentrations, Zn mass fractions and sample size are examined.

Experimental Setup

A scheme of the experimental setup is shown in Figure 1. Experimentation was performed with a 25 mm i.d. quartz tube vertically positioned in a tubular furnace (Carbolite, VST 17/250)), containing a packed-bed of mixtures of Zn and ZnO particles on top of a porous quartz disc. Two type-K thermocouples were placed at the inlet and outlet of the packed-bed. Mixtures of Zn (Sigma-Aldrich, >98%, mean particle dia. 7.9 μm), and ZnO particles (Alpha Aesar, −325 Mesh, 99%, mean particle dia. 0.22 μm) were sieved to remove agglomerates. The total mass flow rate of H_2O and CO_2 was fixed at 300 mL_N/min. Samples of 3,000–9,000 mg were used for the experiments which resulted in packed-bed heights of 0.45–1.65 cm that corresponded to average residence times of 0.139–0.54 s ($T = 678$ K). The Zn mass fraction was varied between 33 and 67 wt % to optimize conversions. A series of experiments was also conducted with 25 wt % Zn-ZnO particles (mean particle dia. 0.97 μm) obtained from the solar thermolysis of ZnO.[4,36] The sample size was ~6,000 mg for all experiments with solar Zn-ZnO mixtures, which resulted in packed-bed heights of ~2.8 cm: more than double the height of a commercial mixture of the same weight, and corresponding to residence times of 3.8 s ($T = 678$ K). Due to lower packing densities, the critical fluidization velocity was decreased and the flow rate was reduced to 80 mL_N/min, to prevent particle entrainment and fluidization. Figure 2 shows SEM pictures of the 50 wt % Zn-ZnO mixture prepared with commercial mixtures (Figure 2a), and of the 25 wt % Zn-ZnO mixture obtained by solar thermolysis of ZnO (Figure 2b). In the commercial sample, smooth solid Zn spheres are surrounded by the submicron ZnO particles. In the solar-made sample, submicron-sized particles of Zn and ZnO create a porous foam structure with high-surface area.

The outlet gas composition was determined by mass spectroscopy (MS, Omnistar GSD301 O: sampling rate = 1 s^{-1}), and gas chromatography (GC, Varian CP-4900 Micro-GC two-channel system: sampling rate 0.5 min^{-1}) after condensing out excess steam. Solid particle characterizations were

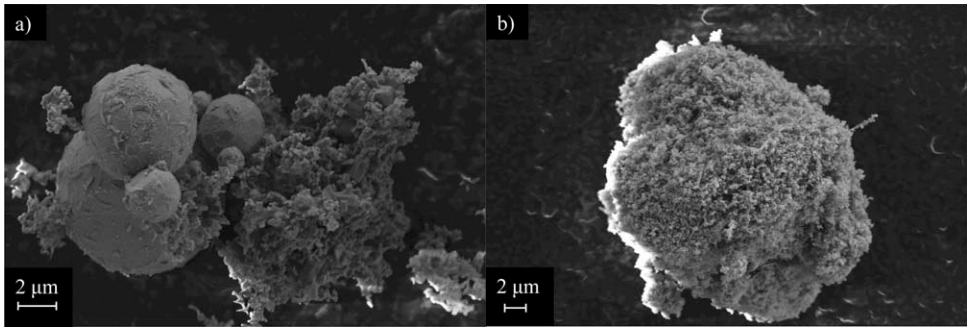

Figure 2. SEM picture of (a) 50 wt % Zn-ZnO mixture prepared with commercial particles, and (b) 25 wt % Zn-ZnO mixture obtained by solar thermolysis of ZnO.

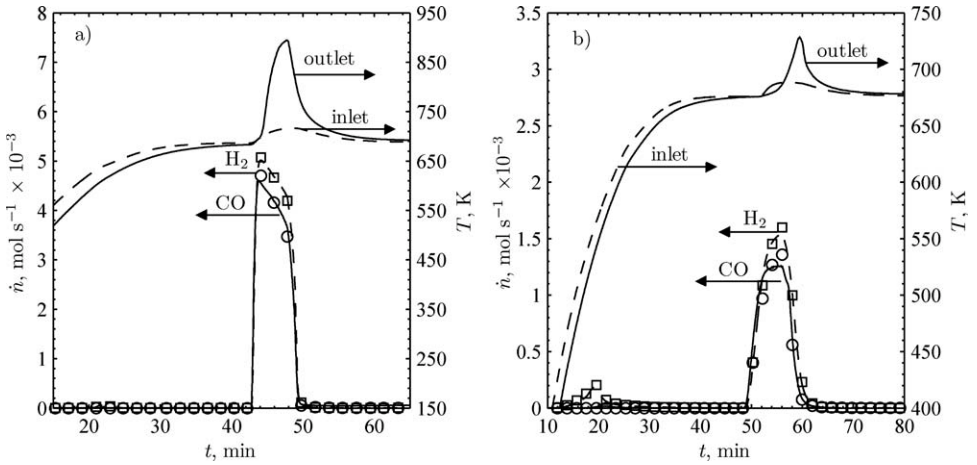

Figure 3. Inlet (dashed) and outlet (solid) temperatures and molar flow rates of CO (circles) and H_2 (squares) as functions of time for representative experimental runs with (a) a 9,000 mg sample of commercial 50 wt % Zn-ZnO exposed to 300 ml_N/min of 50% H_2O–CO_2, and (b) a 6,000 mg sample of solar 25 wt % Zn-ZnO exposed to 80 ml_N/min 50% H_2O-CO_2.

The markers represent the GC measurements, and the lines the fit of the MS data.

performed after each experiment. Zn-to-ZnO conversions were determined by reacting ~500 mg of solid products in 1:1 solution of HCl acid and measuring the pressure change (Newport/Omega, PR33-C-1) due to H_2 production. Scanning electron microscopy (SmartSEM, Carl Zeiss Supra 55VP) was used to examine surface morphologies. Particle-size distributions were analyzed be laser scattering (HORIBA LA-950 analyzer). BET surface areas were determined by N_2 absorption (Micrometrics TriStar 3000).

Results and Discussion

A total of 33 experimental runs were performed for various sample sizes, Zn mass fractions, and reactive gas compositions with commercial and solar Zn/ZnO powder mixtures. Results from two representative runs with a 9,000 mg sample of commercial 50 wt % Zn-ZnO and 6,000 mg sample of solar 25 wt % Zn-ZnO are shown in Figure 3, respectively. The reacting gas in both cases was 50% H_2O-CO_2. O_2 was purged from the system with an Ar flow and the packed-bed was heated to ~680 K. CO_2/H_2O mixtures were then introduced into the system after both the inlet (T_{inlet}, dashed line) and outlet (T_{outlet}, solid line) temperatures stabilized. High concentrations of syngas were immediately detected in the product gases as the gaseous reactants were converted to syngas for 5 min. Nearly complete temporal conversions of H_2O and CO_2 to syngas were observed from $42 < t < 50$ min, and the competitive reaction between H_2O and CO_2 was not observed as reactions were limited by the gaseous reactants and not the available Zn (Figure 3a). The rapid reaction resulted in heat released due to the exothermicity of the reaction, evidenced by a rapid increase in $T_{outlet} = 900$ K. Small increases in T_{inlet} were also observed as heat was conducted through the porous disc. Similar reaction mechanisms with solar 25 wt % Zn-ZnO (Figure 3b), and commercial 50 wt % Zn-ZnO were observed. However, a lower molar flow rate (80 mL_N/min), implemented to prevent particle entrainment, and resulted in a lower syngas production rate and lower peak T_{outlet}. A H_2 peak was observed during the heat-up ($t \approx 20$ min), and can be attributed to moisture in the sample. The reaction nears completion after 10 min

Zn-to-ZnO conversions

The Zn-to-ZnO conversion as a function of time was calculated by coupling high-temporal resolution MS measurements with accurate low-temporal resolution GC measurements for all experiments, except those with 75% H_2O—CO_2 where only GC measurements were used. The Zn-to-ZnO conversions were determined by

$$X_{\text{Zn-to-ZnO}} = \frac{n_{\text{ZnO}}(t)}{n_{\text{Zn,in}}} = \frac{\sum (\dot{n}_{\text{CO}} + \dot{n}_{\text{H}_2})\Delta t}{n_{\text{Zn,in}}} \tag{3}$$

where $n_{\text{Zn,in}}$ and n_{ZnO} denote the initial molar amount of Zn and the molar amount of ZnO produced, respectively, $\dot{n}_{\text{CO}}$, and $\dot{n}_{\text{H}_2}$ are the molar flow rates of CO and H_2, respectively, as determined from the MS and mass flow rate measurements, and Δt is the time increment between measurements. The effects of wt % Zn-ZnO and sample size were also analyzed to maximize $X_{\text{Zn-to-ZnO}}$. Temporal $X_{\text{Zn-to-ZnO}}$ are shown in Figure 4 for 33–67 wt % Zn-ZnO and $m_{\text{sample}} = 3{,}000$ and 9,000 mg. Low $X_{\text{Zn-to-ZnO}}$ were observed with $m_{\text{sample}} = 3{,}000$ mg regardless of Zn wt % as seen with 50 wt % Zn-ZnO (dashed line). Severe sintering and incomplete conversions were observed at the inlet and outlet of the packed-bed and where Zn/ZnO particles were in direct contact with the reactor, resulting in lower $X_{\text{Zn-to-ZnO}}$ with $m_{\text{sample}} = 3{,}000$ mg. Less sintering and incomplete conversions were observed for larger samples as the inlet and outlet areas of the packed-bed accounted for much smaller fractions of the total sample mass. Slower initial conversion rates for $m_{\text{sample}} = 9{,}000$ mg correspond to slower reaction kinetics at the upper layers of the sample. These were initially exposed to lower concentrations of H_2O and CO_2 due to an initial concentration gradient

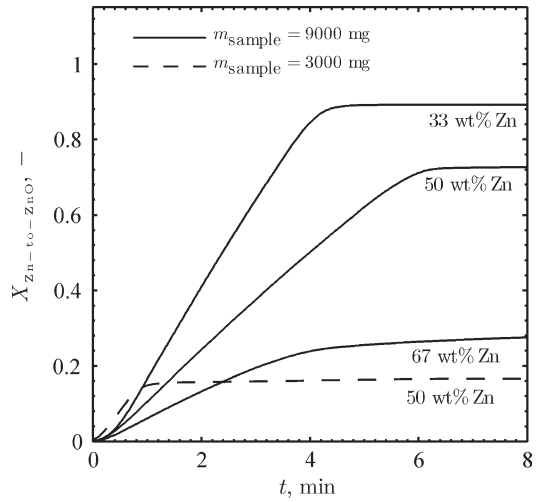

Figure 4. Zn-to-ZnO conversions as a function of time for 50% H_2O-CO_2 with 33, 50, 67 wt % Zn-ZnO and sample sizes of 3,000 and 6,000 mg.

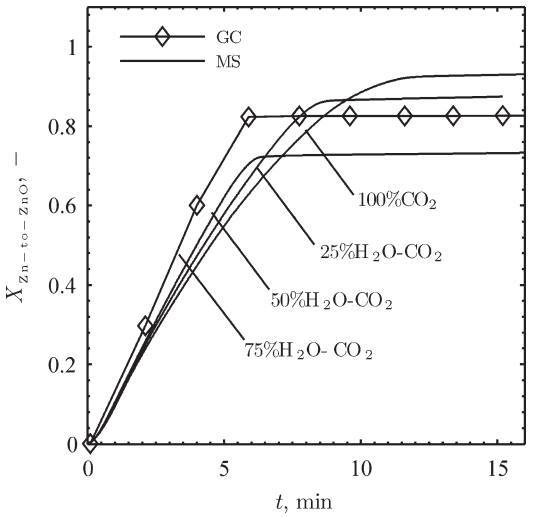

Figure 5. Temporal conversions of Zn-to-ZnO for 50 wt % Zn-ZnO with 25, 50, 75% H_2O-CO_2 and 100% CO_2.

of H_2O and CO_2 caused by high conversions to CO and H_2 at the inlet of the packed-bed. $X_{Zn\text{-}to\text{-}ZnO} = 0.24$ at 67 wt % Zn-ZnO was significantly lower than $X_{Zn\text{-}to\text{-}ZnO} = 0.77$ reported for reducing CO_2,[35] presumably due to higher reaction enthalpies and faster kinetics associated with steam.[26] Furthermore, both $X_{Zn\text{-}to\text{-}ZnO}$ and conversion rates decrease with wt % Zn-ZnO due to a decrease in the available Zn surface area resulting from an insufficient amount of ZnO support that causes agglomeration and sintering. However, when considering the optimal wt % Zn-ZnO, larger amounts of ZnO inert support increase pressure drops and require more sensible heat. For this reason, further investigations were pursued with 50 wt % Zn-ZnO.

The effect of H_2O concentration in the gaseous reactants was examined. Figure 5 shows $X_{Zn\text{-}to\text{-}ZnO}$ as a function of time for wt % 50 Zn-ZnO with 25, 50, 75% H_2O-CO_2 and 100% CO_2. The markers represent the GC measurements which were used for the $X_{Zn\text{-}to\text{-}ZnO}$ calculation of the run with 75% H_2O-CO_2. The results confirm previous observations that increased H_2O(g) concentrations lead to higher reaction rates indicating that the reaction is controlled by similar mechanisms.[26] However, no discernable trends are observed for overall $X_{Zn\text{-}to\text{-}ZnO}$ (0.72–0.91).

Figure 6 shows $\overline{X}_{Zn\text{-}to\text{-}ZnO}$ as a function of inlet gas concentrations for commercial 50 wt % Zn-ZnO with sample sizes of 9,000 mg (circles), and 3,000 mg (diamonds), and for solar 25 wt % Zn-ZnO (squares) with sample sizes of 6,000 mg. The error bars were computed based on individual 95% confidence intervals, and the standard error for the means was 0.069, indicative of good reproducibility between experiments. Variances were due to heterogeneities in the raw Zn and ZnO, in the mixing of the particles, and in the packing of the bed. The individual overall $X_{Zn\text{-}to\text{-}ZnO}$ for the solar samples is presented for two inlet gas concentrations for comparison. Confidence intervals were not added to the plots as experiments were performed only once due to a limited amount of solar Zn. Decreasing the sample size resulted in a significant decrease in $\overline{X}_{Zn\text{-}to\text{-}ZnO}$, well outside the 95% confidence limits of $m_{sample} = 3{,}000$ mg compared with $m_{sample} = 9{,}000$ mg, in agreement with Figure 4. For experiments with 100% CO_2, $\overline{X}_{Zn\text{-}to\text{-}ZnO}$ did not vary significantly with sample mass, consistent with previous observations for reducing CO_2 to CO.[35] The introduction of steam in the system caused a small decrease in $\overline{X}_{Zn\text{-}to\text{-}ZnO}$, also observed in Figure 5, that was within the 95% confidence intervals for $m_{sample} = 9{,}000$ mg but not for $m_{sample} = 3{,}000$ mg. For both sample sizes, further increase of steam concentration caused a decrease in $\overline{X}_{Zn\text{-}to\text{-}ZnO}$ with 50% H_2O-CO_2, and a subsequent increase with 75% H_2O-CO_2, especially pronounced for $m_{sample} = 3{,}000$ mg. This is thought to be

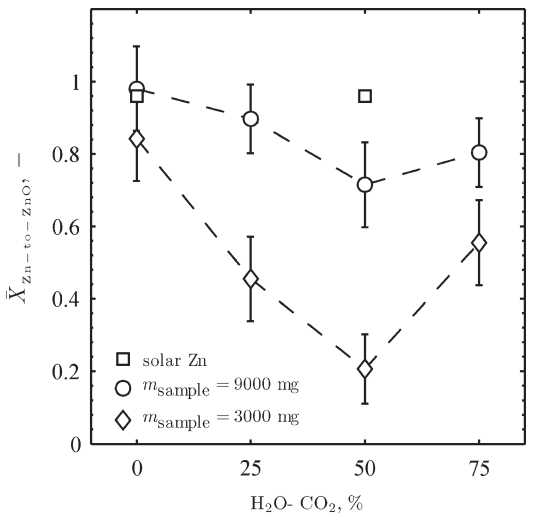

Figure 6. Individual mean Zn-to-ZnO conversions as a function of the % H_2O–CO_2 for commercial 50 wt % Zn-ZnO, with sample sizes of 9,000 mg (circles) and 3,000 mg (diamonds), and for solar 25 wt % Zn-ZnO (squares) with sample sizes of 6,000 mg. Indicated are the error bars based on individual 95% confidence limits.

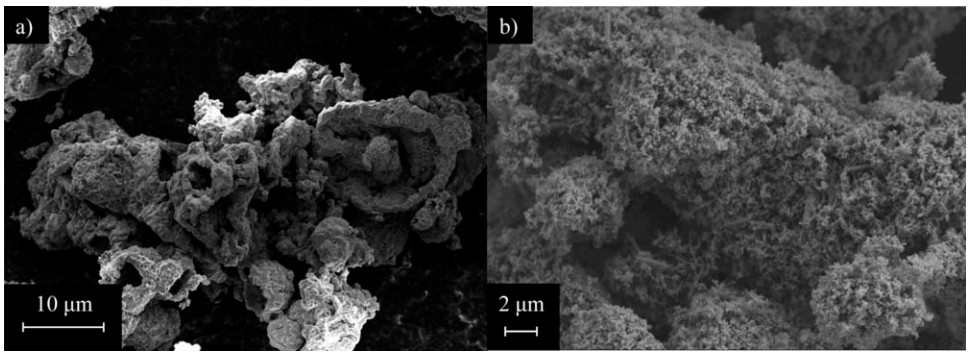

Figure 7. SEM of products collected from the center of the bed after reaction with 50% H_2O-CO_2 for (a) commercial 50 wt % Zn-ZnO, and (b) solar 25 wt % Zn-ZnO.

due to the counteracting phenomena of higher reaction rates, causing more heat released, offset by the formation of more compact ZnO layers and sintering.[26] For 25–50% H_2O-CO_2, the compact oxide layers passivate Zn particles, while at 75% H_2O-CO_2 the thermal stresses resulting from increased kinetics break the ZnO shell, forming cracks and holes and allowing the reaction to proceed. Increased $\overline{X}_{\text{Zn-to-ZnO}}$ for the solar 25% Zn-ZnO is presumably due to the higher residence time, more available surface, more robust inert supports, and lower wt % Zn-ZnO.

Statistical analysis

Analysis of variance was used to compare the effects of Zn mass fraction and gas concentrations on $\overline{X}_{\text{Zn-to-ZnO}}$. Because the interactions between Zn mass fraction and gas concentrations were significant ($p = 0.0094$), individual $\overline{X}_{\text{Zn-to-ZnO}}$ were compared using the Tukey multicomparison procedure.[37,38] Significant differences ($p \leq 0.0254$) between $\overline{X}_{\text{Zn-to-ZnO}}$ were observed for $m_{\text{sample}} = 3{,}000$ mg with 100% CO_2 and 25–75% H_2O-CO_2. There was no significant evidence ($p \geq 0.5099$) to suggest $\overline{X}_{\text{Zn-to-ZnO}}$ differences for $m_{\text{sample}} = 3{,}000$ mg with 100% CO_2 compared with $m_{\text{sample}} = 9{,}000$ mg with 0–75% H_2O-CO_2. $\overline{X}_{\text{Zn-to-ZnO}}$ differences between $m_{\text{sample}} = 9{,}000$ mg with 0–75% H_2O-CO_2 concentrations were not significant except between 100% CO_2 and 50% H_2O-CO_2 ($p = 0.0398$). Significant $\overline{X}_{\text{Zn-to-ZnO}}$ differences ($p \leq 0.0336$) were observed between $m_{\text{sample}} = 3{,}000$ mg and 9,000 mg for 25–75% H_2O-CO_2. The $\overline{X}_{\text{Zn-to-ZnO}}$ for $m_{\text{sample}} = 3{,}000$ mg and 50% H_2O-CO_2 was significantly different ($p \leq 0.0472$) from all other $\overline{X}_{\text{Zn-to-ZnO}}$, indicative of a possible outlier.

Solid characterization

Figure 7 shows the SEM of product samples collected from the middle of the packed-bed after reaction with 50% H_2O-CO_2 for commercial 50 wt % Zn-ZnO (Figure 7a) with $m_{\text{sample}} = 9{,}000$ mg, and for solar 25 wt % Zn-ZnO (Figure 7b). The smooth Zn spheres of Figure 2a reacted to form hollow shells of Figure 7a that adhere to ZnO particles or, in the absence of a ZnO support, sinter together. The nanofilaments of Figure 2b reacted to form a similar porous structure of Figure 7b. The absence of significant sintering after the oxidation of the solar-made Zn corroborates the assumption of a robust support with ZnO.

Figure 8 shows the SEM of sample product for 67 wt % Zn-ZnO (Figure 8a) and 33 wt % Zn-ZnO (Figure 8b) reacting with 50% H_2O-CO_2. The inadequacy of the support led to the passivation of the Zn spheres, whereas increasing the ZnO support resulted to the almost complete conversion.

The BET specific surface areas of the initial Zn and ZnO particles were 2.10 and 5.94 m^2/g, respectively, which decreased to 1.82 m^2/g after the reaction of 25 wt % Zn-ZnO with 50% H_2O-CO_2. The solar Zn had a much higher initial surface area of 21.98 m^2/g, consistent with the highly porous ''sponge-like'' structures observed in the SEM analysis (Figure 2b). After reaction with 50% H_2O-CO_2, the specific surface area decreased to 13.27 m^2/g, indicative of sintering.

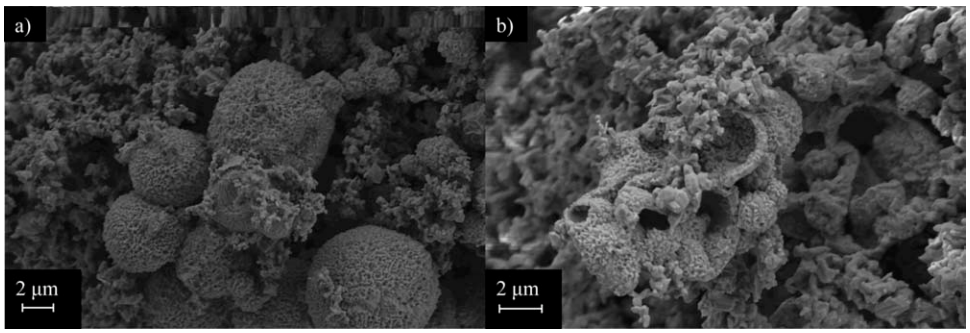

Figure 8. SEM of products collected from the center of the bed after reaction with 50% H_2O-CO_2 for (a) 67 wt % Zn-ZnO, and (b) 33 wt % Zn-ZnO.

Summary and Conclusions

The second, nonsolar step of the Zn/ZnO solar thermochemical cycle to produce syngas from CO_2 and H_2O has been demonstrated in a packed-bed containing Zn/ZnO mixtures. The reaction rate increased with increasing amounts of steam, and overall Zn-to-ZnO conversions of 0.72–0.91 were observed over a range of H_2O/CO_2 concentrations. The H_2/CO ratios in the syngas corresponded to H_2O/CO_2 ratios in the inlet flows. Competitive reactions between the H_2O and CO_2 were not observed as the gaseous flow rate, not solid reactants, limited the reactions. Compared to reactions with pure CO_2, higher reaction rates were observed with H_2O-CO_2 mixtures, which combined with the reaction exothermicity resulted in higher-bed temperatures and local sintering. Zn-ZnO mixtures produced from the solar thermolysis of ZnO were also tested under similar conditions and proved to be highly reactive because of the higher specific surface area, yielding overall Zn-to-ZnO conversions of $\sim$0.96. For optimization and scale-up, a heat-transfer study should be performed to avoid large temperature increases within the bed. The heat release can in principle be recovered to preheat the inlet flows to kinetically favorable temperatures.

Acknowledgments

This work has been financially supported by the Swiss National Science Foundation (contract Nr. 200021-126512) and the BFE - Swiss Federal Office of Energy. The authors thank P. Waffenschmidt at ETH Zurich and A. Frei at PSI for their technical support with the experimental campaigns.

Notation

m = mass
n = molar amount
$\dot{n}$ = molar flow rate
T = temperature
t = time
X = conversion

Abbreviations

FC = flow controller
TC = thermocouple
EV = evaporator
MX = mixer
MS = mass spectrometer
GC = gas chromatograph

Subscripts

in = initial

Literature Cited

1. Service RF. Sunlight in your tank. *Science*. 2009;326:1472–1475.
2. Loutzenhiser PG, Meier A, Steinfeld A. Review of the two-step H_2O/CO_2-splitting solar thermochemical cycle based on Zn/ZnO redox reactions. *Materials*. 2010;3:4922–4938.
3. Nikulshina V, Gebald C, Steinfeld A. CO_2 capture from atmospheric air via consecutive CaO-carbonation and $CaCO_3$-calcination cycles in a fluidized-bed solar reactor. *Chem Eng J*. 2009;146:244–248.
4. Schunk LO, Haeberling P, Wepf S, Wuillemin D, Meier A, Steinfeld A. A receiver-reactor for the solar thermal dissociation of zinc oxide. *Jo Solar Energy Eng*. 2008;130:021009.
5. Schunk LO, Steinfeld A. Kinetics of the thermal dissociation of ZnO exposed to concentrated solar irradiation using a solar-driven thermogravimeter in the 1800–2100 K range. *AIChE J*. 2009;55:1497–1504.
6. Venstrom L, Krueger K, Leonard N, Tomlinson B, Duncan S, Palumbo RD. Solar thermal electrolytic process for the production of Zn from ZnO: An ionic conductivity study. *J Solar Energy Eng*. 2009;131:031005.
7. Wieckert C, Frommherz U, Kraupl S, Guillot E, Olalde G, Epstein M, Santen S, Osinga T, Steinfeld A. A 300 kW solar chemical pilot plant for the carbothermic production of zinc. *J Solar Energy Eng*. 2007;129:190–196.
8. Kodama T, Gokon N. Thermochemical cycles for high-temperature solar hydrogen production. *Chem Rev*. 2007;107:4048–4077.
9. Steinfeld A. Solar thermochemical production of hydrogen–a review. *Solar Energy*. 2005;78:603–615.
10. Perkins C, Weimer AW. Solar-thermal production of renewable hydrogen. *AIChE J*. 2009;55:286–293.
11. Miller J, Allendorf M, Diver R, Evans L, Siegel N, Stuecker J. Metal oxide composites and structures for ultra-high temperature solar thermochemical cycles. *J Mater Sci*. 2008;43:4714–4728.
12. Singh P, Hegde MS. $Ce_{0.67}Cr_{0.33}O_{2.11}$: A new low-temperature O_2 evolution material and H_2 generation catalyst by thermochemical splitting of water. *Chem Mater*. 2009;22:762–768.
13. Chueh WC, Falter C, Abbott M, Scipio D, Furler P, Haile SM, Steinfeld A. High-flux solar-driven thermochemical dissociation of CO_2 and H_2O using nonstoichiometric ceria. *Science*. 2010;330:1797–1801.
14. Charvin P, Abanades S, Flamant G, Lemort F. Two-step water splitting thermochemical cycle based on iron oxide redox pair for solar hydrogen production. *Energy*. 2007;32:1124–1133.
15. Fresno F, Fernández-Saavedra R, Belén Gómez-Mancebo M, Vidal A, Sánchez M, Isabel Rucandio M, Quejido AJ, Romero M. Solar hydrogen production by two-step thermochemical cycles: Evaluation of the activity of commercial ferrites. *Int Hydrogen Energy*. 2009;34:2918–2924.
16. Roeb M, Sattler C, Kluser R, Monnerie N, Oliveira Ld, Konstandopoulos AG, Agrafiotis C, Zaspalis VT, Nalbandian L, Steele A, Stobbe P. Solar hydrogen production by a two-step cycle based on mixed iron oxides. *J Solar Energy Eng*. 2006;128:125–133.
17. Ishihara H, Kaneko H, Hasegawa N, Tamaura Y. Two-step water-splitting at 1273–1623 K using yttria-stabilized zirconia-iron oxide solid solution via co-precipitation and solid-state reaction. *Energy*. 2008;33:1788–1793.
18. Clarke JA, Fray DJ. Oxidation of zinc vapour by hydrogen-water vapour mixtures. *Trans Inst Min Metall Sec C*. 1979;88:C161–C166.
19. Lv M, Zhou J, Yang W, Cen K. Thermogravimetric analysis of the hydrolysis of zinc particles. *Int J Hydrogen Energy*. 2010;35:2617–2621.
20. Ma X, Zachariah MR. Size-resolved kinetics of Zn nanocrystal hydrolysis for hydrogen generation. *Int Hydrogen Energy*. 2010;35:2268–2277.
21. Chambon M, Abanades S, Flamant G. Kinetic investigation of hydrogen generation from hydrolysis of SnO and Zn solar nanopowders. *Int Hydrogen Energy*. 2009;34:5326–5336.
22. Ernst FO, Steinfeld A, Pratsinis SE. Hydrolysis rate of submicron Zn particles for solar H_2 synthesis. *Int J Hydrogen Energy*. 2009;34:1166–1175.
23. Vishnevetsky I, Epstein M. Production of hydrogen from solar zinc in steam atmosphere. *Int Hydrogen Energy*. 2007;32:2791–2802.
24. Loutzenhiser PG, Gálvez ME, Hischier I, Stamatiou A, Frei A, Steinfeld A. CO_2 splitting via two-step solar thermochemical cycles with Zn/ZnO and FeO/Fe_3O_4 redox reactions II: Kinetic analysis. *Energy Fuels*. 2009;23:2832–2839.
25. Stamatiou A, Loutzenhiser PG, Steinfeld A. Solar syngas production via H_2O/CO_2-splitting thermochemical cycles with Zn/ZnO and FeO/Fe_3O_4 redox reactions. *Chem Mater*. 2009;22:851–859.
26. Stamatiou A, Loutzenhiser PG, Steinfeld A. Solar syngas production from H_2O and CO_2 via two-step thermochemical cycles based on Zn/ZnO and FeO/Fe_3O_4 redox reactions: Kinetic analysis. *Energy Fuels*. 2010;24:2716–2722.
27. Hamed TA, Venstrom L, Alshare A, Brulhart M, Davidson JH. Study of a quench device for the synthesis and hydrolysis of Zn nanoparticles: Modeling and experiments. *J Solar Energy Eng*. 2009;131:031018.

28. Melchior T, Piatkowski N, Steinfeld A. H_2 production by steam-quenching of Zn vapor in a hot-wall aerosol flow reactor. *Chem Eng Sci*. 2009;64:1095–1101.
29. Ernst FO, Tricoli A, Pratsinis SE, Steinfeld A. Co-synthesis of H_2 and ZnO by *in situ* Zn aerosol formation and hydrolysis. *AIChE J*. 2006;52:3297–3303.
30. Weiss RJ, Ly HC, Wegner K, Pratsinis SE, Steinfeld A. H_2 production by Zn hydrolysis in a hot-wall aerosol reactor. *AIChE J*. 2005;51:1966–1970.
31. Loutzenhiser PG, Gálvez ME, Hischier I, Graf A, Steinfeld A. CO_2 splitting in an aerosol flow reactor via the two-step Zn/ZnO solar thermochemical cycle. *Chem Eng Sci*. 2010;65:1855–1864.
32. Wegner K, Ly HC, Weiss RJ, Pratsinis SE, Steinfeld A. In situ formation and hydrolysis of Zn nanoparticles for H_2 production by the 2-step ZnO/Zn water-splitting thermochemical cycle. *Int Hydrogen Energy*. 2006;31:55–61.
33. Funke HH, Diaz H, Liang X, Carney CS, Weimer AW, Li P. Hydrogen generation by hydrolysis of zinc powder aerosol. *Int J Hydrogen Energy*. 2008;33:1127–1134.
34. Berman A, Epstein M. The kinetics of hydrogen production in the oxidation of liquid zinc with water vapor. *Int J Hydrogen Energy*. 2000;25:957–967.
35. Loutzenhiser PG, Barthel F, Stamatiou A, Steinfeld A. CO_2 reduction with Zn particles in a packed-bed reactor. *AIChE J*. 2010;n/a–n/a.
36. Villasmil W. *Design of a 100 kW Reactor for the Solar Thermal Dissociation of Zinc Oxide*. Zurich, Switzerland: ETH Zurich; 2010.
37. JMP 8. SAS Institute, Inc. Cary, NC; 2008.
38. Neter J, Kutner MH, Nachtsheium CJ, Wasserman W. *Applied Linear Statistical Models*. Boston, MA: WCD McGraw-Hill; 1996.

Manuscript received Dec. 31, 2010, and revision received Jan. 20, 2011.